Imaging the injured beating heart intravitally and the vasculoprotection afforded by haematopoietic stem cells

Kavanagh, Dean; Lokman, Adam; Neag, Georgiana; Colley, Abigail; Kalia, Neena

DOI:
10.1093/cvr/cvz118

Imaging the injured beating heart intravitally and the vasculoprotection afforded by haematopoietic stem cells

Dean P.J. Kavanagh* (PhD), Adam Lokman* (MBBS), Georgiana Neag (MRes), Abigail Colley (MRes), Neena Kalia (PhD)

Institute of Cardiovascular Sciences, College of Medical and Dental Sciences, University of Birmingham, B15 2TT, UK

*** Joint First Authors**

Short Title : Intravital imaging of beating IR injured heart

Subject Codes: Basic Science Research, Myocardial Infarction, Imaging, Platelets/Thrombosis, Inflammation, Stem Cells

Correspondence to:

Dr Neena Kalia
Institute of Cardiovascular Sciences,
College of Medical and Dental Sciences,
University of Birmingham,
B15 2TT, UK

Tel: +44 (0) 121 414 8818,
Email: n.kalia@bham.ac.uk

ABSTRACT

Rationale: Adequate microcirculatory perfusion, and not just opening of occluded arteries, is critical to salvage heart tissue following myocardial infarction (MI). However, the degree of microvascular perfusion taking place is not known, limited primarily by an inability to directly image coronary microcirculation in a beating heart *in vivo*. Haematopoietic stem/progenitor cells (HSPCs) offer a potential therapy but little is known about their homing dynamics at a cellular level and whether they protect coronary microvessels. This study used intravital microscopy (IVM) to image the anaesthetised mouse beating heart microcirculation following stabilisation.

Methods/Results: A 3D-printed stabiliser was attached to the ischaemia-reperfusion injured (IRI) beating heart. The kinetics of neutrophil, platelet and HSPC recruitment, as well as functional capillary density (FCD), was imaged post-reperfusion. Laser speckle contrast imaging (LSCI) was used for the first time to monitor ventricular blood flow in beating hearts. Sustained hyperaemic responses were measured throughout reperfusion, initially indicating adequate flow resumption. IVM confirmed large vessel perfusion but demonstrated poor transmission of flow to downstream coronary microvessels. Significant neutrophil adhesion and microthrombus formation occurred within capillaries with the latter occluding them, resulting in patchy perfusion and reduced FCD. Interestingly, 'patrolling' neutrophils were also observed in capillaries. HSPCs readily trafficked through the heart but local retention

was poor. Despite this, remarkable anti-thromboinflammatory effects were observed, consequently improving microvascular perfusion.

Conclusion: We present a novel approach for imaging multiple microcirculatory perturbations in the beating heart with LSCI assessment of blood flow. Despite deceptive hyperaemic responses, increased microcirculatory flow heterogeneity was seen, with non-perfused areas interspersed with perfused areas. Microthrombi, rather than neutrophils, appeared to be the major causative factor. We further applied this technique to demonstrate local stem cell presence is not a pre-requisite to confer vasculoprotection. This is the first detailed *in vivo* characterisation of coronary microcirculatory responses post-reperfusion injury.

Key words – coronary microcirculation, ischaemia-reperfusion injury, intravital microscopy

INTRODUCTION

Treatment of myocardial infarction (MI) focuses on rapidly re-establishing reperfusion following blockage in one or more of the coronary arteries. Despite successful thrombolytic and primary percutaneous coronary interventions (PCI), a significant proportion of patients still incur muscle damage and proceed to develop heart failure.[1-2] Indeed, restoration of normal epicardial blood vessel flow following PCI, but with sub-optimal myocardial perfusion, can be observed in as high as 50% of patients.[3-4] This is strongly associated with larger infarcts, reduced ventricular function and overall worse outcomes than in patients with full perfusion recovery.[5-6] It is likely that in the absence of overt atherosclerotic disease or occlusions within larger and clinically visible conduit vessels, tissue damage occurs subsequent to inadequate coronary microcirculatory perfusion. Indeed, in recent years, cardiovascular magnetic resonance (CMR) imaging has provided new insights into the significant impact microvascular obstruction and intramyocardial haemorrhage has on clinical outcomes.[7] Furthermore, progressive loss of distal perfusion at the tissue level and neutrophil accumulation has been demonstrated in patients post-MI using PET scanning.[8] However, current clinical imaging tools such as x-ray angiography, CMR and PET cannot spatially resolve blood vessels less than 200μm in diameter and so are unable to image small capillaries nor the blood cells within them at a cellular level.

An inability to directly image microvessels of the heart has led to cardiologists focussing their efforts on improving flow within the angiographically visible part of the coronary circulation. This has prevented a complete identification of the role of the microcirculation in ischaemic cardiovascular disease. The microcirculation comprises the functional ‘business’ end of the circulation and, in the heart, is responsible for 75% of myocardial blood flow. The significant oxygen demand of the heart is provided by an extensive dense network of capillaries running between all muscle fibres providing almost every fibre with its own capillary. The microvasculature controls total coronary resistance and is thus critical in regulating myocardial blood flow. Moreover, it is highly responsive to, and a vital participant in, the inflammatory response. Dysfunction of the coronary microvasculature has recently emerged as a potentially important mechanism contributing to MI with important prognostic implications. Indeed, an increasing number of publications have emphasised the need to focus research interests into studying the coronary microcirculation from both a basic and clinical perspective and prevent it remaining as a research ‘black box’.[9-12] The importance of the microcirculation in heart disease is further exemplified in conditions such as microvascular angina (cardiac syndrome X) and in MI with non-obstructive coronary arteries (MINOCA) where patients present with the clinical features of an acute MI but without angiographic evidence of obstructive coronary arteries. [12-14]

Currently, little is known about the full range of microcirculatory responses to MI *in vivo*, limited primarily by an inability to directly image these events in a beating heart. Functional readouts, such as blood flow and pressure, can be determined clinically using a Doppler flow wire inserted into the coronary artery or assessed using thrombolysis in MI (TIMI) flow or myocardial blush. However, these assessments are mainly of larger vessels and actual visualisation of coronary microcirculation, let alone any detrimental events taking place within them, remains impossible with current clinical imaging tools. Experimental knowledge to date has commonly been obtained histologically, but these static snapshots provide no indication of the real-time kinetics of inflammatory cell recruitment - a dynamic process - in the presence of pathophysiological flow. Tissue sections also do not offer any information on microvessel integrity and perfusion. Consequently, experts have recently suggested creating an international "coronary microcirculatory observatory", a virtual facility utilising imaging techniques such as intravital microscopy (IVM) to properly interrogate the coronary microcirculation in the beating heart of living animals.[11]

However, real-time microscopic imaging of the beating heart has been very challenging as motion compromises spatial and temporal resolution and therefore requires 'stabilisation' of the heart – this in itself is technically very difficult. We have developed a stabilisation method that sufficiently reduces motion in a small region of the beating left ventricle to permit intravital imaging of the coronary microcirculation. Li and colleagues have used a somewhat similar approach to monitor dynamic neutrophil events in a donor beating heart transplanted in the neck of a recipient.[15] However, we present further novel data illustrating the extensive nature of neutrophil and platelet adhesion that occurs in the microcirculation following myocardial ischaemia-reperfusion injury (IRI) in a native heart *in situ*. In particular, we show platelet microthrombi occluding significant lengths of the capillaries and the considerable detrimental impact of these occlusions on functional capillary density (FCD). Furthermore, we combine IVM with full field laser speckle contrast microscopy to correlate microvascular events with whole beating heart blood perfusion. Importantly we show poor microcirculatory perfusion is observed intravitally despite an overall reactive hyperaemic response detected using laser speckle imaging. Increased clinical recognition of the importance of the coronary microcirculation has meant identifying strategies to improve detrimental perturbations within it has also gained recent attention. To this effect, we also investigated the homing of systemically delivered exogenous bone marrow (BM)-derived haematopoietic stem/progenitor cells (HSPCs) to the injured heart. This is the first study to directly image, at a cellular level, the myocardial homing and trafficking of any exogenous stem cell type *in vivo*. We demonstrate their remarkable ability to confer vasculoprotection, and have elucidated potential therapeutic mechanisms of action, which occurs despite limited interactions with the coronary microcirculation and poor myocardial retention.

METHODS

Myocardial IR injury

Experiments were conducted on male C57BL/6 mice (8-12 weeks) in accordance with the Animals (Scientific Procedures) Act of 1986 (ASPA) which enforces Directive 2010/63/EU of the European Parliament on the protection of animals used for scientific purposes (Project licence: P552D4447). We have previously reported the microcirculatory response to IRI, and HSPC trafficking, within the liver, gut and kidney of male mice. In order to make meaningful comparisons between these events in different vascular beds, the current work was also performed in male mice. Anaesthesia was induced by I.P. administration of ketamine hydrochloride (100mg/kg) and medetomidine hydrochloride (100mg/kg) and maintained as required via intra-arterial administration. Mice were intubated and ventilated with medical oxygen via a MiniVent rodent ventilator (stroke volume: 220µl, respiratory rate: 130pm; Biochrom Ltd. Harvard Apparatus, UK). The carotid artery was cannulated to facilitate infusion of fluorescently labelled cells, antibodies, dyes and maintenance anaesthetic. IRI

was induced by ligating the left anterior descending (LAD) artery for 45mins with reperfusion initiated for 2hrs by removal of the suture.

Haematopoietic stem / progenitor cells – HPC-7 cells

Intravital studies monitoring HSPC trafficking have been limited due to difficulties in isolating sufficient numbers for *in vivo* experimentation. Therefore, an immortalised HSPC line, HPC-7, was used. These cells have characteristics similar to primary cells including surface expression of common murine HSC markers (c-kit$^+$, CD34$^-$, Lin$^-$) and surface adhesion molecules and are also able to reconstitute haematopoiesis when injected into lethally irradiated hosts.[16] We have previously used HPC-7s to model hepatic and intestinal HSPC recruitment.[17-20] To image HPC-7s, they were labelled with 5μM carboxyfluorescein diacetate succinimidyl ester (CFDA-SE; Life Technologies, UK) as previously described.[17-20] To assess whether their adhesion could be enhanced in the heart *in vivo*, HPC-7s were pre-treated with hydrogen peroxide (H_2O_2, 100μM; 1hr) prior to infusion. This strategy has previously been used by us to successfully enhance HSPC retention in the gut.[18]

Characterising injury on coronary endothelium and myocytes using flow cytometry

Flow cytometry on digested heart cells was developed to determine whether coronary microvasculature was more susceptible to IRI than myocytes and whether HSPCs could modify inflammatory and oxidative injury. Ventricles were mechanically digested using collagenase type-I dispersion solution (0.1%; Wako Chemicals, Japan) and strained through a 70μm filter into media (DMEM, 10% FCS, 1% penicillin/streptomycin; Sigma). Cells were isolated by centrifugation, fixed, permeablised with 70% ethanol and then re-suspended in blocking agent (rat anti-mouse CD16/32 antibody; BioLegend). Washed cells were incubated with antibodies as required: PE-conjugated rat anti-mouse CD31 (dilution 1:50; 390; ThermoFisher Scientific), PE-conjugated rat IgG2a control (dilution 1:50; eBR2a; ThermoFisher Scientific), PE-conjugated human anti-mouse/human/rat cardiac Troponin-T (cTnT; dilution 1:10; REA400; Miltenyi Biotec), Alexa 488 conjugated rat anti-mouse ICAM-1 (1:50), PE-Cy7 anti-mouse VCAM-1 (1:50), PE-conjugated human REA control (dilution 1:10; REA293; Miltenyi Biotec), purified polyclonal goat anti-8-OHdG (dilution 1:500; Abcam), purified goat IgG control (dilution 1:500, Abcam). Data analysis was performed on washed cells using FACSCalibur (BD Biosciences). Adhesion molecule expression and oxidative damage on cTnT$^+$ myocytes and CD31$^+$ ECs was quantitated in 30,000 cellular events and expressed as mean fluorescence intensity.

8-OHdG and DHE staining of vena cava endothelial cells *in vitro*

The ability of HSPCs to modify oxidative damage or limit the generation of superoxide species within cardiovascular endothelial cells (EC) following ROS challenge was assessed *in vitro*. Immortomouse derived vena cava ECs (VCEC)[17] were grown to confluence and then exposed to H_2O_2 (100μM) to oxidatively damage them for 24 or 72 hrs in the presence or absence of $5x10^4$ HSPCs. To assess oxidative damage, ethanol fixed and permeabilised VCECs were incubated with a polyclonal goat anti-mouse 8-OHdG antibody (dilution 1:500) followed by Alexa 488-conjugated donkey anti-goat IgG antibody (dilution 1:250). Dihydroethidium (DHE; 500μl; 10μM) was added to detect superoxide generation. Cells were imaged using EVOS and integrated density was calculated for 8-OHdG and DHE.

Intravital imaging of the cardiac microcirculation

To facilitate intravital visualisation of epicardial microcirculation in the anaesthetised mouse beating heart, we modified a stabiliser previously described by Lee and colleagues.[21] A small 3D-printed ring, with internal and external diameters of 2.25mm and 4mm respectively, was lowered onto the left ventricle using a micromanipulator. It was permanently fixed to the

heart using a thin layer of clinical grade Vetbond (3M UK plc, Bracknell, UK) on its underside. This sufficiently reduced motion of a small region of the ventricle to allow imaging within its centre whilst the rest of heart continued to beat normally. No BP/HR changes were identified as a result of this process as determined by photoplethysmograghy (**Supplementary Figure 1**). The central area was kept moist by application of 0.9% saline with the surrounding area covered with saran wrap to prevent loss of moisture. In IRI hearts, application of the stabiliser was initiated five minutes after the LAD artery was unclamped and downstream of the ligation site (area most at risk of infarction). The same region was identified in sham hearts. Intravital imaging was performed using a Nipkow spinning disk confocal head attached to an upright Olympus BX61WI microscope with an Evolve EMCCD camera (Photometrics, USA). Since it took ~20-30mins before the mouse was ready for imaging, the first recording lasting 2min took place from a pre-selected field of view at 30 mins post-reperfusion. Subsequent 2min recordings were made from the same area every 15 mins for 2hrs. All data was captured, stored and analysed using Slidebook 6 software (Intelligent Imaging Innovations, USA).

To image endogenous neutrophils and platelets in the same mouse, 20µl of PE-conjugated rat anti-mouse Gr-1 antibody (RB6-8C5; Thermofisher) and an APC-conjugated rat anti-mouse CD41 antibody (MWReg30, Thermofisher) were both administered 5mins prior to ischaemia. Platelet aggregates/microthrombi were quantitated by placing a mask around CD41 positive areas and integrated fluorescence density, which took into account size and flourescence intensity, was calculated. Considering the sheer numbers of endogenous platelets, labelling all of them made it difficult to quantitate singular platelet events. Therefore, in separate mice, $1x10^8$ CFSE-labelled donor platelets were systemically injected. This results in a labelled fraction in the recipient of ~5% of all circulating platelets, a value low enough to allow individual platelets to be imaged. To investigate the kinetics of HSPC homing to the heart, 100µL of $2x10^6$ CFSE-labelled HSPCs were injected at 30min post-reperfusion. This time point enabled stabiliser attachment, mouse transfer to the microscope and HSPC 'first-pass' to be imaged. However, to assess potential vasculoprotective effects, HSPCs were injected within 5mins of reperfusion. Neutrophils, platelets and HSPCs were manually counted and considered adherent if they remained static for >30 seconds. Free flowing cells were identified as those that passed through the coronary microcirculation without making adhesive interactions. To identify areas of perfused blood vessels, 100µl of FITC-BSA (Sigma, UK) was administered at 2hrs post-reperfusion. All intravital data was analysed by an independent blinded observer. At the end of experimentation, mice were culled by cervical dislocation.

Laser speckle contrast imaging (LSCI) of the beating mouse heart

LSCI was utilised to quantitate left ventricular myocardial blood flow. Mice were surgically prepared as described earlier but no stabiliser was attached. An LSCI device (moorFLPI-2; Moor Instruments, UK) was positioned above the exposed heart. A demarked area, typically downstream of the LAD ligation site, was identified for collection of flux data during pre-ischaemia, ischaemia and at every 15mins post-reperfusion. A total number of 1000 frames were captured at each time point using the manufacturer supplied image software (mFLPI2Measure V2.0; mFLPIReview V5.0) at a frame rate of 25Hz and using spatial processing (sliding window, time constant: 0.1s). *Basic Speckle Analysis software* (SpAn), written in-house (available on request), allowed identification and collation of flux values during diastole for each time point (**Supplementary Figure 2)**.

Measurement of serum inflammatory cytokine concentrations

Circulating cytokine concentrations were identified in serum samples from mice following sham surgery, IRI, or IRI+HSPC administration within 5 minutes of reperfusion. Reperfusion was performed for 1hr. Serum was isolated by centrifugation (2,000rpm, 10 mins). Samples were loaded in triplicate onto a Bio-Plex pro mouse cytokine 23-plex assay plate (Bio-Rad Laboratories, CA, US) and analysed using a Luminex 200 plate reader (Bio-Rad Laboratories, CA, US) following the manufacturer's instructions.

Statistical analysis

All statistical analysis was performed using Graphpad Software (GraphPad Software, Inc., USA). Direct comparisons between two groups were performed using a Student t-test. Comparisons between three or more groups were performed by one-way ANOVA, followed by Sidak post-hoc tests. For time course studies, such as neutrophil recruitment over time, comparisons were made by two-way ANOVA, followed by Sidak post-hoc tests for individual time points. All data is presented as mean±SEM.

RESULTS

Neutrophil recruitment and platelet microthrombus formation increases rapidly following myocardial IRI

The number of neutrophils freely circulating through coronary microcirculation increased at all time points post-reperfusion when compared to sham hearts, but this did not attain statistical significance (**Fig.1A**). Interestingly, numbers of adherent neutrophils within sham hearts was high with ~60-70 cells observed per field of view. However, this more than doubled following IRI and remained significantly ($p<0.0001$) elevated (**Fig.1B&F**). No change in the number of individual, free flowing platetets occurred as a result of injury (**Fig.1C**). Unlike neutrophils, their adhesion within sham hearts was minimal, but significantly ($p<0.01$) increased following injury (**Fig.1D**). IRI also led to the striking and significant ($p<0.001$) formation of numerous platelet aggregates and microthrombi within coronary capillaries which was sustained throughout the duration of the experiment (**Fig.1E&F**). No such aggregates were identified in sham hearts.

Adherent neutrophils do not compromise blood flow unlike platelet microthrombi

Since significant adherent neutrophils were observed in sham hearts, it was possible that the process of placing the stabiliser induced a local inflammatory response. Therefore, sham experiments were conducted mice in which the beating heart was imaged in the absence of the stabiliser. Although images were difficult to obtain, blurry and relatively out-of-focus, adherent neutrophils were still present in similar numbers to those seen in stabilised hearts (**Fig.2A**). They did not compromise blood flow as evidenced by FITC-BSA perfused capillaries being visible in the whole field of view (**Fig.2B&3A**). IRI induced a marked and significant increase in individual neutrophil adhesion, although neutrophil clusters were also identified (**Fig.2C**). Blood flow was compromised in IRI hearts as evidenced by a failure of some capillaries to load with FITC-BSA (**Fig.2D&3B**). Interestingly, these areas did not correspond with neutrophil adhesion, but rather predominantly matched areas in which striking adherent platelet aggregates and microthrombi were identified. These were occlusive and often identified upstream of areas in which no FITC-BSA was observed (**Fig.2D&E)**. Microthrombi were not generally observed in the larger vessels but formed primarily within coronary capillaries often occupying significant lengths of vessel. Numerous smaller and more rounded platelet aggregates were also found dispersed within the field of view. Aggregates were often, but not always, comprised of both neutrophils and platelets.

These aggregates appeared to occassionaly 'block' the circulation of trafficking neutrophils (**Fig.2F**). Although adherent neutrophils appeared at first glance to be completely stationary, detailed analysis of videos demonstrated that some neutrophils, in both sham and IRI hearts, were actually moving short distances or 'patrolling' the length of the capillary (**Fig.2G**).

Myocardial IRI is associated with impaired capillary perfusion

An extensive network of FITC-BSA perfused capillaries was observed in sham mice, paralleling the arrangement of muscle fibres, with cross connections along their length. Focussing up and down on the field of view showed no areas devoid of perfused capillaries. Well perfused medium-sized vessels were also visible in some fields of view (**Fig.3A**). In contrast, IRI was associated with multiple areas in which FITC-BSA did not perfuse. This resulted in patchy areas that appeared devoid of any microvasculature, indicating poor FCD. Indeed, in some fields of view, up to half the imaged area appeared non-perfused. Furthermore, the structured parallel arrangement of capillaries was lost with the microvasculature appearing more disorganised. Accumulation of FITC-BSA, identified as slightly wider vascular areas of intense fluorescence, was also seen along the length of some capillaries. Interestingly, medium sized vessels were still readily visible and well perfused in injured hearts (**Fig.3B**).

Despite poor HSPC retention within injured hearts, significant vasculoprotective effects are identified

Approximately 20-30 free flowing HSPCs were identified at all time points in sham mice. However, in IRI hearts, this number increased almost 4-fold at 30mins post-reperfusion (the first time point after infusion). At all other time points, although circulating HSPC numbers remained elevated, the effect was not as remarkable. H_2O_2 pre-treatment did not enhance HSPC homing to the injured heart. (**Fig.4A**). Adhesion was low and did not differ between IRI and sham hearts nor with pre-treatment (**Fig.4B-C**). HSPC infusion did not affect circulating neutrophil numbers but did remarkably and significantly decrease neutrophil ($p<0.0001$) and platelet ($p<0.001$) adhesive events in IRI hearts (**Fig.4D-G**). This resulted in clear improvements in capillary FITC-BSA perfusion (**Fig.4H**). Since H_2O_2 did not influence HSPC homing, the vasculoprotective effects of pre-treated cells was not tested.

Myocardial IRI induced a sustained ventricular hyperaemic response

Left ventricular diastolic and systolic events were easily detected on flux analysis recordings as high and low points respectively. We focussed on diastolic events for comparative purposes (**Fig.5A**). In sham mice, blood flow did not change throughout the course of imaging. As expected, ischaemia reduced flow with arbitrary flux values decreasing from ~1700 to ~1400. Reperfusion was associated with a significant ($p<0.001$) and sustained reactive hyperaemic response with values increasing to ~2000 (**Fig.5B**). The presence of HSPCs in IRI hearts produced blood flow flux recordings that were statistically ($p<0.05$) different to sham hearts but did not differ from IRI hearts not receiving HSPCs.

Myocardial endothelial cells are more susceptible to oxidative stress than cardiomyocytes following acute IRI but this injury can be reduced by HSPCs

Digested whole heart cells were examined using flow cytometry and $CD31^+$ ECs and $CTnT^+$ myocytes identified (**Fig.6A**). The percentage of myocytes recovered from the sampled population of cardiac cells was consistently higher (~80%) than the yield of ECs (~10%) across all groups of mice (**Fig.6B**). Compared to sham controls, ICAM-1 expression on ECs was significantly increased during ischaemia ($p<0.05$) and reperfusion ($p<0.01$). This increase was reduced in mice receiving HSPCs when compared to IRI mice not receiving

cellular therapy (**Fig.6C**). Interestingly, VCAM-1 and oxidative stress ($p<0.01$) only increased during reperfusion with both returning to baseline values in mice receiving HSPCs (**Fig.6D&E**). Although there was a trend for myocytes to also undergo oxidative damage following injury, this did not reach statistical significance. Furthermore, only ~1-2% of myocytes presented with oxidative damage compared to ~30% of ECs (**Fig.6F**).

Microvascular endothelial oxidative stress can be reduced in the presence of HSPCs *in vitro*

The ability of HSPCs to decrease oxidative stress, specifically in cardiovascular ECs *in vitro*, was tested in a co-culture system using VCECs. Oxidative damage resulting from H_2O_2 treatment, determined by 8-OHdG staining, was not reduced following incubation with HSPCs for 24hr but was significantly ($p<0.05$) reduced by 72hr (**Fig.7A**). H_2O_2 driven ROS generation, measured by DHE staining, was also reduced at 72hr ($p<0.001$) following incubation with HSPCs (**Fig.7B&C)**.

HSPCs significantly decreased serum levels of multiple pro-inflammatory cytokines but increased levels of IL-10

IRI induced a significant ($p<0.05$) increase in the circulating serum levels of 10 out of 23 inflammatory cyokines tested (**Table 1**). Greater than 6-fold increases were observed in IL-6, IL-12, G-CSF, KC, MCP-1 and MIP-1β levels. HSPCs reduced the serum concentration of 9 of these factors as well as some cytokines whose increase post-IRI was not significantly increased. Interestingly, HSPCs significantly ($p<0.01$) increased the serum levels of IL-10.

DISCUSSION

Adequate microcirculatory perfusion, and not just opening of an occluded epicardial artery, is critical in order to salvage myocardial tissue post-MI. However, the pathophysiological changes in coronary microvascular perfusion taking place following an ischaemic insult have not previously been imaged directly. Here, we present a novel approach to image multiple coronary microcirculatory perturbations intravitally in a stabilised beating mouse heart with assessment of overall blood flow using laser speckle imaging. A sustained ventricular hyperaemic response was noted throughout reperfusion. On its own, this could have been interpreted as blood flow being adequately re-established to repay the debt acquired during ischaemia. However, it was clear from intravital studies that this was poorly transmitted to coronary capillaries and thus did not correspond to adequate perfusion at a microvascular level.

Neutrophil adhesion increased rapidly in injured hearts, doubling by 30mins post-reperfusion. Neutrophil capture is generally confined to post-capillary venules due to their high and preferential expression of endothelial adhesion molecules.[22] In the heart, we noted neutrophil retention mainly within capillaries, a region of the vasculature not usually associated with cellular recruitment. VCAM-1 expression was also increased in IRI vasculature. However, unlike in previously published work,[23] this was observed on capillaries as well as larger vessels. This suggests active capture mechanisms may also be involved in mediating capillary-neutrophil interactions in the heart. Neutrophil accumulation has long been recognized histologically as a significant component of myocardial IRI. However, the impact of their sequestration on coronary perfusion has not been possible to determine from static sections. Intravitally, we show that obstructions in microvessel blood flow do not generally occur in areas with individual adherent neutrophils. This was evidenced by the fact that FCD did not decrease in the whole field of view in parallel with the

diffuse neutrophil adhesion. Indeed, only distinct patchy areas lacking FITC-BSA perfusion were observed.

Interestingly, a significant population of adherent neutrophils were observed in sham hearts *in vivo*. This was unusual based on our extensive intravital experience of imaging other solid organs.[15-19] Adhesion many have been stimulated by attaching the stabiliser but this is unlikely as they this population was present even in non-stabilised hearts. We speculate that some trafficking neutrophils may have become trapped as blood vessels were compressed during systole. Extravascular compression during isovolumetric contraction markedly reduces coronary flow.[24-26] Indeed, LSCI clearly identified decreased myocardial blood flow during systole. As far as we are aware, this is the first application of LSCI to the beating mouse ventricle and demonstration of real-time phasic changes associated with the cardiac cycle. Interestingly, adherent neutrophils did not obstruct blood flow as evidenced by the ease and ability of FITC-BSA to permeate through the sham heart microvasculature.

Numbers of free-flowing neutrophils circulating through the injured heart also doubled throughout reperfusion. This is an interesting observation, particularly in light of the fact that the density of FITC-BSA perfused capillaries decreased. Higher numbers of circulating neutrophils passing through less microvasculature can be explained by a possible increase in the blood flow to the injured heart. Indeed, this is supported by the LSCI data. Reactive hyperaemic responses post-occlusion benefit the oxygen-deprived myocardium. However, these responses also inadvertently introduce more inflammatory cells into an environment primed for their adhesion.

We also occasionally observed neutrophils, in both sham and injured hearts, that appeared to slowly ‘patrol' short lengths of the capillary. This patrolling behaviour is novel in the heart and the physiological relevance is unclear in sham mice, but following IRI it may possibly reflect attempts to identify emigration sites. Recent intravital imaging provides evidence that neutrophils also constitutively patrol glomerular capillaries and following injury exhibit a greater dwell time and increased ROS generation.[27] ‘Crawling’ neutrophils, seeking to provide the first line of defense against infection, have also been identified in pulmonary capillaries.[28] Collectively, these studies provide insights into a new neutrophil behaviour that does not appear to be site-specific.

Although individual platelet adhesion was enhanced, it was the formation and sustained elevated presence of platelet aggregates that was a striking feature in reperfused hearts. Numerous small, rounded aggregates were seen as well as larger, elongated microthrombi occupying significant lengths of the capillaries. The major consequence of these was the detrimental effect on capillary perfusion in their immediate vicinity. This was demonstrated by the lack of FITC-BSA presence downstream of microthrombi. Hence multiple non-perfused areas were identified interspersed with perfused microvasculature. Although it is often suggested that platelet microaggregates impede microvascular flow following MI[29-30], our studies provide the first direct *in vivo* evidence of their occlusive nature in an IR injured beating heart.

A marked but transient increase in blood delivery to the heart following ischaemia, lasting only a few minutes, has been demonstrated both experimentally and clinically.[31-32] Indeed in humans, coronary blood flow can increase up to five times basal flow to meet increased demand following release of a variety of vasodilatory factors.[31] Interestingly, in the current study a more sustained reactive hyperaemic response was identified. This discrepancy may possibly be explained by technical differences. Previously, blood flow responses were measured from one of the major coronary arteries using an inserted Doppler flow guide wire. However, in the current study, the full-field optical nature of LSCI was able to image a larger ventricular area, thus averaging macro- and microvascular flow changes, over longer periods of time.

Although individual neutrophils did not appear to hinder flow, their increased presence is detrimental. Since activated neutrophils generate ROS, their rapid and high capillary presence increases the susceptibility of these delicate structures to early and significant

oxidative damage. Indeed, flow cytometry data demonstrated coronary endothelium, rather than myocytes, was the primary and initial target of oxidative injury. Furthermore, a high degree of correlation between capillary CD31 and 8-OHdG immunostaining was noted histologically. Others have also shown this differential susceptibility to injury with endothelial and cardiomyocyte apoptotic death occurring at 5 and 60mins respectively in isolated perfused hearts.[33-34] Collectively, this data highlights coronary microcirculation as an early and principal therapeutic target to prevent ensuing muscle damage.

Our model was therefore used for the first time to image stem cell trafficking *in vivo* at a cellular level and, importantly, ascertain whether vasculoprotection was a critical therapeutic mechanism. We focussed on cellular therapy as there has been intense interest in their use for cardiovascular diseases. Even through the field has progressed rapidly to clinical trials, it is agreed that more basic research is required to understand their mechanisms of action and thus improve on their modest clinical success. Although clinical studies have primarily used total un-fractionated BM mononuclear cells (comprising HSPCs, mesenchymal stem cells (MSCs), lymphocytes and monocytes), we focused on a purified population of HSPCs. A 4-fold increase in circulating HSPCs was identified in IRI hearts, which may be related to the hyperaemic response. However, 25-30 circulating cells were consistently observed throughout reperfusion. This was unusual as we have shown in other organs that HSPCs were only observed on the 'first pass' immediately after infusion and not thereafter.[16-18,20] Surprisingly, these homing events did not result in any dramatic local HSPC retention, which remained low and similar to sham hearts. Furthermore, pre-treatment strategies did not modify their adhesion. Poor retention is a well described phenomenon. For example, Hoffman and colleagues demonstrated <2.6% retention of unselected BM-derived cells in STEMI patients when delivered 5-10 days after stenting.[35] Pulmonary entrapment is a common feature of cellular therapy[36-37] which we also noted in the current study.

This observation was potentially troublesome, as the efficacy of cellular therapy has been thought to be dependent on sufficient retention within injury sites.[38] Indeed, a recent study demonstrated that developing platelet-based strategies to improve the targeted delivery of peripheral blood mononuclear cells to the IRI heart led to reduced infiltration of inflammatory cells, reduced fibrosis and enhanced capillary density after IR injury.[39] However, we showed that despite limited local retention, HSPCs afforded rapid and remarkable vasculoprotection in the injured heart, limiting both neutrophil and platelet adhesion and thus improving FCD. BM-derived stem and progenitor cells can secrete a rich and potent combination of growth factors and anti-inflammatory cytokines that act in a paracrine manner on neighbouring cells.[40-41] Even without retention in the heart, these factors may be released systemically from remote sites and confer vasculoprotection in the heart.[36] Indeed, remote transplantation of MSCs into the interscapular region protected the IRI heart.[42] Since HSPCs continuously circulated through the heart, it is also possible they became activated to release paracrine factors locally as they trafficked through the injured coronary microcirculation. HSPCs inhibited both a number of pro-inflammtory cytokines as well as ICAM-1/VCAM-1 up-regulation, which could mechanistically explain the decreased neutrophil infiltration. Interestingly, we show that HSPCs also induced a significant increase in circulating IL-10 levels in IRI mice. IL-10 is a naturally occurring, potent anti-inflammatory cytokine which can suppress secretion of various pro-inflammatory cytokines both *in vitro* and *in vivo* via inhibition of NF-κβ.[43] A number of immunohistochemical studies have demonstrated that exogenous IL-10 can suppress myocardial inflammation as evidenced by decreased neutrophil infiltration in similar injury models.[44-45] Indeed, the beneficial effects of remote ischaemic pre-conditioning in the heart have also been demonstrated to be mediated via increases in IL-10.[46] Furthermore, genetically engineering mesenchymal stem cells (MSC) to overexpress IL-10 has been shown to better reduce infarct size and cardiac impairment compared to individual treatments of MSC or IL-10 administration [47] It is therefore likely that increased serum levels of IL-10 in mice receiving HSPCs mechanistically explains the vasculoprotective effects observed in the current study.

The impact on platelet activity is somewhat harder to explain. It is possible that platelet aggregation occurred subsequent to endothelial damage and denudation instigated by neutrophils. However, since both thrombotic and inflammatory events had already occurred by the earliest imaging time point, it is not clear which cellular event occurred first. Alternatively, HSPCs may possess direct anti-thrombotic potency. Indeed, this was recently described for MSCs in the lungs and was linked to modification of urokinase-type plasminogen activator, a protein important in early thrombi resolution.[48-49] Whether HSPCs modify this pathway is not known and would require further examination. The only event not influenced by HSPCs was hyperaemia, which is perhaps not surprising, as this is a reactive response to ischaemia which was induced in all experimental groups including mice receiving cellular therapy.

Spinning disk confocal allowed for high resolution and real-time capture of dynamic images of the beating heart that would not have been possible with conventional single laser raster scanning microscopy. However, the imaging is relatively 'superficial' with an imaging depth of ~25-35μm beneath the heart surface. Theoretically, confocal imaging could have delivered signals from more depth. However, our low exposure times, required for video-rate imaging of coronary microvessels, limited imaging depth. Greater depth could be achieved with multiphoton microscopy. However, our initial attempts using multiphoton intravital microscopy (Olympus Fluoview) have been challenging due to residual movement that remains even after stabilisation (unpublished data) and additional methodological enhancements are required such as respiratory/cardiac gating. Even so, we find imaging depth in the heart to be modestly increased to ~70-80μm. To appreciate the global effects of myocardial IRI on the coronary microcirculation throughout the muscle wall, multiphoton imaging on tissue sections spanning the full thickness of the ventricular wall is required.

To summarise, intravital imaging of the beating mouse heart, combined with laser speckle microscopy, provides a wealth of dynamic information on the coronary microcirculation that is not possible to obtain with conventional immunohistological approaches. We show for the first time that although IRI is associated with an overall hyperaemic response in the injured ventricle, this may be deceptive as at a microvascular level, increased flow heterogeneity exists due to occluded coronary capillaries. Hence there exists a great mismatch between a "global hyperaemic response" during reperfusion, and microcirculatory heterogeneity. To the best of our knowledge, this is the first detailed *in vivo* characterisation of multiple microcirculatory perturbations taking place in the IR injured beating heart. Although Li and colleagues have also intravitally imaged a beating mouse heart, they imaged a donor heart transplanted in the neck of the recipient, with a focus on neutrophil kinetics.[15] Crucially, our research is conducted on the native heart *in situ* which has greater clinical relevance as an experimental model for MI. We further show that local stem cell presence is not a pre-requisite to preventing myocardial thromboinflammatory events. Since acellular delivery of stem cell-derived paracrine factors may be sufficient to activate repair mechanisms, this should be tested in our model and is indeed the basis of future studies. It is anticipated that this model will have a number of future applications. For example, microvascular dysfunction is a key feature of cardiovascular disease in females, with both cardiac syndrome X and MINOCA being more common in women. Applying our beating heart intravital imaging method to female mice would be a worthwhile pursuit to assess sex related differences in the microcirculatory responses to IR injury.

FUNDING / ACKNOWLEDGMENTS

The authors thank the British Heart Foundation (PG/14/92/31234) for funding part of this work. The authors would also like to thank Siobhan Young and the Clinical Immunology Service at the University of Birmingham for their help with the Luminex assay.

CONFLICT OF INTEREST

None

REFERENCES

1. Kelly DJ, Gershlick T, Witzenbichler B, Guagliumi G, Fahy M, Dangas G, Mehran R, Stone GW. Incidence and predictors of heart failure following percutaneous coronary intervention in ST-segment elevation myocardial infarction: the HORIZONS-AMI trial. *Am Heart J.* 2011;162663-70.
2. Cowie MR, Lacey L, Tabberer M**.** Heart failure after myocardial infarction: a neglected problem? *Br J Cardiol.* 2005;12:205-8.
3. De Maria GL, Cuculi F, Patel N, Dawkins S, Fahrni G, Kassimis G, Choudhury RP, Forfar JC, Prendergast BD, Channon KM, Kharbanda RK, Banning AP. How does coronary stent implantation impact on the status of the microcirculation during primary percutaneous coronary intervention in patients with ST-elevation myocardial infarction? *Eur Heart J.* 2015;36:3165-77.
4. Ito H, Maruyama A, Iwakura K, Takiuchi S, Masuya- ma T, Hori M, Higashino Y, Fujii K, Minamino T. Clinical implications of the “no reflow” phenomenon. A predictor of complications and left ventricular remodeling in reperfused anterior wall myocardial in-farction. *Circulation* 1996;93:223-228.
5. Bolognese L, Carrabba N, Parodi G, Santoro GM, Buonamici P, Cerisano G, Antoniucci D. Impact of microvascular dysfunction on left ventricular remodeling and long-term clinical outcome after primary coronary angioplasty for acute myocardial infarction. *Circulation* 2004*;*109:1121-1126.
6. Camici P, Crea F. Coronary microvascular dysfunction. *N Engl J Med* 2007; 356:830-40.
7. Bulluck H, Dharmakumar R, Arai AE, Berry C, Hausenloy DJ. Cardiovascular magnetic resonance in acute ST-segment-elevation myocardial infarction: recent advances, controversies, and future directions. *Circulation* 2018; 137:1949-1964.
8. Thackeray JT, Derlin T, Haghikia A, Napp LC, Wang Y, Ross TL, Schäfer A, Tillmanns J, Wester HJ, Wollert KC, Bauersachs J, Bengel FM. Molecular imaging of the chemokine receptor CXCR4 after acute myocardial infarction. *JACC Cardiovasc Imaging* 2015; 8:1417-1426.
9. Lüscher TF. From epicardial coronary arteries to the coronary microcirculation: novel insights into a neglected issue. *Eur Heart J.* 2017;38:461–464
10. Sambuceti G, L'Abbate A, Marzilli M. Why should we study the coronary microcirculation? *Am J Physiology - Heart Circ Phys.* 2000;279:H2581-H2584.
11. Pries & Reglin. Coronary microcirculatory pathophysiology: can we afford it to remain a black box? *Eur Heart J.* 2016;38:478-488.
12. Crea F, Camici PG, Bairey Merz CN. Coronary microvascular dysfunction: an update. *Eur Heart J*. 2014;35:1101-11.
13. Chandrasekaran B, Kurbaan AS. Myocardial infarction with angiographically normal coronary arteries. *J R Soc Med*. 2002;95:398-400.
14. Agewall S, Beltrame JF, Reynolds HR, Niessner A, Rosano G, Caforio AL, De Caterina R, Zimarino M, Roffi M, Kjeldsen K, Atar D, Kaski JC, Sechtem U, Tornvall P. ESC working group position paper on myocardial infarction with non-obstructive coronary arteries. *Eur Heart J.* 2017;38:143-153.
15. Li W, Nava RG, Bribriesco AC, Zinselmeyer BH, Spahn JH, Gelman AE, Krupnick AS, Miller MJ, Kreisel D. Intravital 2-photon imaging of leukocyte trafficking in beating heart. *J Clin Invest*. 2012;122:2499-508.
16. Pinto do Ó, Richter PK, Carlsson L. Hematopoietic progenitor/stem cells immortalized by Lhx2 generate functional hematopoietic cells *in vivo. Blood* 2002;99:3939-3946.
17. Kavanagh DP, Durant LE, Crosby HA, Lalor PF, Frampton J, Adams DH, Kalia N. Haematopoietic stem cell recruitment to injured murine liver sinusoids depends on (alpha)4(beta)1 integrin/VCAM-1 interactions. *Gut* 2010;59:79-87.
18. Kavanagh DP, Yemm AI, Alexander JS, Frampton J, Kalia N. Enhancing the adhesion of hematopoietic precursor cell integrins with hydrogen peroxide increases recruitment within murine gut. *Cell Transplant.* 2013;22:1485-99.

19. Kavanagh DP, Yemm AI, Zhao Y, Frampton J, Kalia N. Mechanisms of adhesion and subsequent actions of a haematopoietic stem cell line, HPC-7, in the injured murine intestinal microcirculation *in vivo. PLoS One* 2013;8:e59150.
20. White RL, Nash G, Kavanagh DPJ, Savaga COS, Kalia N. Modulating the adhesion of haematopoietic stem cells with chemokines to enhance their recruitment to the ischaemically injured murine kidney. *PLoS One* 2013;8(6):e66489.
21. Lee S, Vinegoni C, Feruglio PF, Fexon L, Gorbatov R, Pivoravov M, Sbarbati A, Nahrendorf M, Weissleder R. Real-time *in vivo* imaging of the beating mouse heart at microscopic resolution. *Nat Comm*. 2012;3:1054
22. Ley K. Molecular mechanisms of leukocyte recruitment in the inflammatory process. Cardiovas Res. 1996;32:733-742
23. Bowden RA, Ding ZM, Donnachie EM, Petersen TK, Michael LH, Ballantyne CM, Burns AR. Role of alpha4 integrin and VCAM-1 in CD18-independent neutrophil migration across mouse cardiac endothelium. *Circ Res*. 2002;90:562-9.
24. Panerai RB, Chamberlain JH, Sayers BM. Characterization of the extravascular component of coronary resistance by instantaneous pressure-flow relationships in the dog. *Circ Res.* 1979:45(3):378-90
25. Sabbah HN, Marzilli M, Liu ZQ, Stein PD. Coronary extravascular compression influences systolic coronary blood flow. *Heart Vessels* 1986;2140-6.
26. Sabiston DC, Gregg DE. Effect of cardiac contraction on coronary blood flow. *Circulation* 1957;15:14-20.
27. Devi S, Li A, Westhorpe CL, Lo CY, Abeynaike LD, Snelgrove SL, Hall P, Ooi JD, Sobey CG, Kitching AR, Hickey MJ. Multiphoton imaging reveals a new leukocyte recruitment paradigm in the glomerulus*. Nat Med.* 2013;19:107-12.
28. Harding MG, Zhang K, Conly J, Kubes P. Neutrophil crawling in capillaries; a novel immune response to *Staphylococcus aureus*. *PLoS Pathog.* 2014;10:e1004379.
29. Pachel C, Mathes D, Arias-Loza AP, Heitzmann W, Nordbeck P, Deppermann C, Lorenz V, Hofmann U, Nieswandt B, Frantz S. Inhibition of platelet GPVI protects against myocardial ischemia-reperfusion injury. *Arterioscler Thromb Vasc Biol*. 2016,36(4):629-35.
30. Katoh Y, Iwabuchi K, Hayashi I, Konishi H, Itoh S, Okumura K, Ra C, Nagaoka I, Daida H. Platelets activated by collagen through the immunoreceptor tyrosine-based activation motif in the Fc receptor gamma-chain play a pivotal role in the development of myocardial ischemia-reperfusion injury. *J Mol Cell Cardiol.* 2005;39:856-64.
31. Olivercrona GK, Gotberg M, Harnek J, Wang L, Jacobson KA, Erlinge D. Coronary artery reperfusion: The ADP receptor P2Y1 mediates early reactive hyperemia *in vivo* in pigs. *Purinergic Signalling* 2004;1:59-64
32. Vassalli G, Hess OM. Measurement of coronary flow reserve and its role in patient care. *Basic Res Cardiol* 1998;93:339-53
33. Singhal A K, Symons J D, Boudina S, Jaishy B , Shiu YT. Role of endothelial cells in myocardial ischemia-reperfusion injury. *Vasc Dis Prev.* 2010;7:1-14
34. Scarabelli T, Stephanou A, Rayment N, Pasini E, Comini L, Curello S, Ferrari R, Knight R, Latchman D. Apoptosis of endothelial cells precedes myocyte cell apoptosis in ischemia/reperfusion injury. *Circulation* 2001;104:253-6.
35. Hofmann M, Wollert KC, Meyer GP, Menke A, Arseniev L, Hertenstein B, Ganser A, Knapp WH, Drexler H. Monitoring of bone marrow cell homing into the infarcted human myocardium. *Circulation* 2005;111:2198-2202.
36. Ziegler M, Haigh K, Nguyen T, Wang X, Lim B, Yap ML, Eddy EM, Haigh JJ, Peter K. The pulmonary microvasculature entraps induced vascular progenitor cells (iVPCs) systemically delivered after cardiac ischemia-reperfusion injury: Indication for preservation of heart function via paracrine effects beyond engraftment. *Microcirculation* 2018; 21:e12493.
37. Fischer UM, Harting MT, Jimenez F, Monzon-Posadas WO, Xue H, Savitz SI, Laine GA, Cox CS Jr. Pulmonary passage is a major obstacle for intravenous stem cell delivery: the pulmonary first-pass effect. *Stem Cells Dev* 2009; 18:683-92.

38. Chavakis E, Urbich C, Dimmeler S. Homing and engraftment of progenitor cells: a prerequisite for cell therapy. *J Mol Cell Cardiol*. 2008; 45:514-*522.*
39. Ziegler M, Wang X, Lim B, Leitner E, Klingberg F, Ching V, Yao Y, Huang D, Gao XM, Kiriazis H, Du XJ, Haigh JJ, Bobik A, Hagemeyer CE, Ahrens I, Peter K. Platelet-targeted delivery of peripheral blood mononuclear cells to the ischemic heart restores cardiac function after ischemia-reperfusion injury. *Theranostics* 2017, 7:3192-3206.
40. Korf-Klingebiel M, Kempf T, Sauer T, Brinkmann E, Fischer P, Meyer GP, Ganser A, Drexler H, Wollert KC. Bone marrow cells are a rich source of growth factors and cytokines: implications for cell therapy trials after myocardial infarction. *Eur Heart J.* 2008; 29:2851-2858.
41. Ziff OJ, Bromage D, Yellon DM, Davidson SM. Therapeutic strategies utilizing SDF-1α in ischaemic cardiomyopathy. *Cardiovasc Res*. 2018; 114:358-367.
42. Preda MB, Rønningen T, Burlacu A, Simionescu M, Moskaug JØ, Valen G. Remote transplantation of mesenchymal stem cells protects the heart against ischemia-reperfusion injury. *Stem Cells* 2014; 32(8):2123-34.
43. Saxena A, Khosraviani S, Noel S, Mohan D, Donner T, Hamad AR. Interleukin-10 paradox: A potent immunoregulatory cytokine that has been difficult to harness for immunotherapy. *Cytokine* 2015; 74:27-34.
44. Krishnamurthy P, Rajasingh J, Lambers E, Qin G, Losordo DW, Kishore R. IL-10 inhibits inflammation and attenuates left ventricular remodeling after myocardial infarction via activation of STAT3 and suppression of HuR. *Circ Res.* 2009; 104:e9-18.
45. Jung M, Ma Y, Iyer RP, DeLeon-Pennell KY, Yabluchanskiy A, Garrett MR, Lindsey ML. IL-10 improves cardiac remodeling after myocardial infarction by stimulating M2 macrophage polarization and fibroblast activation. *Basic Res Cardiol.* 2017; 112(3):33.
46. Cai ZP, Parajuli N, Zheng X, Becker L. Remote ischemic preconditioning confers late protection against myocardial ischemia-reperfusion injury in mice by upregulating interleukin-10. *Basic Res Cardiol.* 2012; 107(4):277.
47. Meng X, Li J, Yu M, Yang J, Zheng M, Zhang J, Sun C, Liang H, Liu L. Transplantation of mesenchymal stem cells overexpressing IL10 attenuates cardiac impairments in rats with myocardial infarction. J Cell Physiol. 2018; 233(1):587-595.
48. Peng X, Li J, Yu X, Tan R, Zhu L, Wang J, Wang R, Gu G, Liu Q, Ren L, Wang C, Hu Q. Therapeutic effectiveness of bone marrow-derived mesenchymal stem cell administration against acute pulmonary thromboembolism in a mouse model. *Thromb Res.* 2015;135(5):990-9.
49. Santo SD, Tepper OM, von Ballmoos MW, Diehm N, Völzmann J, Baumgartner I, Kalka C. Cell-based therapy facilitates venous thrombus resolution. *Thromb Haemo* 2009;101:460-464.

Table

Table 1. HSPCs reduce serum concentration of multiple pro-inflammatory factors but increase sreum levels of IL-10, a known anti-inflammatory cytokine. IRI induced a significant increase in the circulating serum levels of 10 out of 23 inflammatory cyokines tested using a Luminex cytokine array kit. Greater than 6-fold increases were observed in IL-6, IL-12, G-CSF, KC, MCP-1 and MIP-1β levels. HSPCs reduced the serum concentration of 9 of these factors as well as some cytokines whose increase post-IRI was not significantly increased. HSPC administration significantly ($p<0.01$) increased the serum levels of interleukin-10. *† $p<0.05$, **†† $p<0.01$, ***††† $p<0.001$; Sham vs IR injury or IR injury with HSPCs. One-tailed students t-test, n>9

Cytokine	Sham – pg/ml	IR injury – pg/ml	IR injury + HSCs – pg/ml
Interleukin-1α	14.07 ± 2.90	18.62 ± 3.95	10.63 ± 0.67 †
Interleukin-1β	37.18 ± 5.06	42.84 ± 4.37	24.94 ± 2.40 ††
Interleukin-2	14.92 ± 3.00	11.65 ± 0.86	8.17 ± 0.48 ††
Interleukin-3	17.13 ± 2.45	16.46 ± 1.67	10.93 ± 0.93 ††
Interleukin-4	13.61 ± 3.48	10.27 ± 2.77	6.76 ± 4.29
Interleukin-5	32.63 ± 11.95	31.56 ± 5.69	17.78 ± 2.91 †
Interleukin-6	316.138 ± 118.21	1993.53 ± 841.45 *	425.07 ± 78.19 †
Interleukin-9	51.29 ± 7.54	45.76 ± 4.83	34.22 ± 2.64 †
Interleukin-10	143.57 ± 9.06	222.70 ± 45.84 *	452.48 ± 41.06 †††
Interleukin-12(p40)	2253.75 ± 350.50	14588.86 ± 5889.30 *	2424.66 ± 179.39 †
Interleukin-12(p70)	501.84 ± 85.43	555.36 ± 57.31	350.24 ± 38.07 ††
Interleukin-13	278.182 ± 51.10	337.87 ± 38.67	159.26 ±25.87 †††
Interleukin-17	18.70 ± 2.68	14.50 ± 1.22	11.36 ± 1.06 †
Eotaxin	992.67 ± 113.83	1607.58 ± 50.43 *	1020.15 ± 90.44 †††
G-CSF	395.23 ± 97.79	2720.72 ± 1272.80 *	200.29 ± 36.04 †
GM-CSF	54.52 ± 7.25	61.95 ± 6.50	41.09 ± 4.75 ††
IFNγ	46.44 ± 7.28	42.25 ± 4.50	30.55 ± 2.20 †
KC (IL-8)	326.15 ± 93.22	1769.48 ± 783.47 *	227.52 ± 28.93 †
MCP-1	638.92 ± 121.67	5016.62 ± 2117.35 *	704.97 ± 93.02 †
MIP-1α	21.84 ± 8.95	48.51 ± 21.69	37.30 ± 10.35
MIP-1β	169.46 ± 56.60	1545.83 ± 736.81 *	250.28 ± 58.80 †
RANTES	108.06 ± 15.03	248.96 ± 79.09 *	85.75 ± 10.29 †
TNFα	191.95 ± 29.16	369.49 ± 95.21 *	154.62 ± 19.28 †

Figure Legends

Figure 1. Neutrophil recruitment and microthrombus formation increases rapidly following myocardial IRI. (A) Free flowing neutrophil number does not increase following IRI when compared to sham controls (n=5/group). **(B)** Neutrophil adhesion within sham hearts is high but increases following IRI (****p<0.0001 IR vs Sham with significant differences at all time pionts; n=5/group). **(C)** Free flowing donor platetets transitting through myocardium is not increased following IRI (n=5/group). **(D)** Singular donor platelet adhesion increases across the imaging period following IRI (**p<0.01 IR vs Sham; n=5/group). **(E)** Accumulation of endogeous platelets, appearing as platelet aggregates and microthrombi increases following IRI and is quantitated as integrated fluorescence density (***p<0.001 IR vs Sham with significant differences at all time points; n=5/group). 2-way ANOVA with Sidak's multiple comparison test used for all analyisis. **(F)** Representative intravital images of the beating mouse heart to show rapid accumulation and gradual increases of both neutrophils and platelets. Neutrophils present primarily as individual cells with platelets found as aggregates or microthrombi. Merged images show aggregates comprised of both cell types (yellow). Green: Neutrophils (PE+anti-Gr-1ab); Red: endogenous platelets (APC+anti-CD41ab). Scale bars represent 100μm.

Figure 2. Neutrophils adherent within sham hearts do not prevent blood flow – platelet aggregates main contributors to occlusive events in IRI. (A) Blurry and out-of-focus intravital images obtained from 'non-stabilised' hearts, but still showing adherent neutrophils in sham myocardial microcirculation. Better quality and easily quantifiable intravital images obtained following stabilisation, which confirm neutrophil adhesion in beating sham hearts. **(B)** Adherent neutrophils in sham hearts do not compromise blood flow as widespread FITC-BSA perfused capillaries are visible. Green: neutrophils (PE+anti-Gr-1ab); Red: FITC-BSA. **(C)** IRI increases neutrophil adhesion, most of which are singular, although aggregates also identified. **(D)** Blood flow compromised in IRI hearts as evidenced by not all capillaries being filled with FITC-BSA. This did not always correspond to areas of neutrophil adhesion. Some capillaries 'finish' abruptly (arrowhead; out-of-focus large vessel seen in this field of view). Magnified image (right) shows neutrophils often adherent or trapped within platelet microthrombi in injured hearts, as indicated by co-staining, to form large occlusive aggregates. These impact detrimentally on blood flow as indicated by inability of FITC-BSA (red) to perfuse into capillaries (*) downstream of microthrombus (blue/green - circle) comprised of platelets (blue) and neutrophils (green). **(E)** Neutrophil adhesion, platelet aggregation and microthrombus formation following IRI. Microthrombi occupy and follow the contours of a significant length of the capillary (*). Co-localisation (yellow) indicates aggregates are often, but not always, comprised of both neutrophils and platelets. Green: neutrophils (PE+anti-Gr-1ab); Red: endogenous platelets (APC+anti-CD41ab). **(F)** Time-lapse images from an IRI beating heart video. From left to right, within the white circles, a single circulating neutrophil (green, N) is shown unable to move down the capillary as it is occluded by a downstream stationary platelet thrombus (red, t). * = circulating neutrophils seen in one frame but not the next. **(G)** Time lapse images from a sham beating heart showing a 'patrolling' neutrophil. Dotted lines - track movement of 'patrolling' neutrophil. Scale bars represent 100μm

Figure 3. Myocardial IRI is associated with significantly impaired capillary perfusion and a disturbed microvascular organisation. FITC-BSA was administered 2hrs post-reperfusion and representative intravital images are shown. **(A)** In sham mice, an extensive network of FITC-BSA perfused capillaries can be observed. Most capillaries parallel the arrangement of the muscle fibres with cross connections that run obliquely to fibres along their length. Although the stabiliser is attached to avoid visible large coronary arteries, well perfused medium-sized vessels can be seen in some fields of view (out of focus in some of the images). **(B)** IRI is associated with multiple areas in which FITC-BSA does not perfuse, resulting in visualisation of patchy areas devoid of any vasculature (*). In some fields of

view, at least half the imaged area appears non-perfused. The organised parallel arrangement of capillaries is lost with microvasculature appearing 'disorganised'. Accumulation of FITC-BSA, identified as wider areas of intense fluorescence, occasionally seen along the length of some capillaries (arrowheads). Interestingly, medium sized vessels are still perfused and thus readily visible. Scale bars represent 100µm.

Figure 4. Despite poor HSPC retention within IRI hearts, vasculoprotective effects are identified. **(A)** 20-30 free flowing HSPCs observed circulating through myocardial microvessels at all time points in sham mice. However, in IRI hearts, an almost 4-fold increase is noted at 30mins post-reperfusion. Pre-treatment of HSPCs with H_2O_2 does not enhance their homing to injured heart. **(B)** Adhesion of naïve or pre-treated HSPCs is not increased as a result of injury but gradually rises in all groups. **(C)** Representative intravital images shows a similar retention of intra-arterially injected exogenous CFSE-labelled HSPCs in all groups. **(D)** HSPCs do not affect the free flow of neutrophils through the injured heart but do decrease **(E)** neutrophil adhesion (****p<0.0001 vs IR with significant differences at all timepoints; n≥4). **(F)** Presence of platelet aggregates and microthrombi is also significantly reduced (***p<0.001 vs IR with significant differences at all timepoints; n≥4). 2-way ANOVA with Sidak's multiple comparison test used for all analyisis. **(G)** Representative intravital images of injured heart showing a reduction in endogenous neutrophils and platelet presence when compared non-treated injured hearts. Green: neutrophil (PE+anti-Gr-1ab); Red: endogenous platelets (APC+anti-CD41ab). **(H)** Improvement in capillary perfusion subsequent to cellular therapy as determined using FITC-BSA. Scale bars represent 100µm.

Figure 5. Laser speckle contrast imaging (LSCI) reveals a sustained reactive myocardial hyperaemia in response to IRI. (A) Photos of the beating mouse heart are shown alongside the corresponding full field LSCI flux heat map. All flux images have been normalised on the same palette settings. Pre-ischaemia hearts are well perfused as indicated by a more yellow/red heat map. As expected, flow is reduced in the ischemic heart resulting in heat maps that are primarily blue. Reperfusion induces a rapid and striking hyperaemic response as indicated by mostly red heat maps. Analysis graphs from SpAN rendered data show diastolic and systolic events captured as high points (green circles) and low points respectively. In these representative analysis graphs, arbitrary flux values decrease from ~1700 to ~1400 as a result of ischaemia and increase to ~2000 after reperfusion. **(B)** This raw data has been presented as mean normalised flow flux. In sham mice, ventricular blood flux does not change throughout the course of imaging. Ischaemia decreases this value. Reperfusion induces a rapid and sustained reactive hyperaemic response. The presence of HSpCs in IRI mice produces flux recordings statistically different to sham hearts but no different to IRI hearts not receiving HSPCs. ****p<0.0001, $^{+}$p<0.05; ANOVA with Sidak's multiple comparison test; n=3/group.

Figure 6. Myocardial endothelial cells are more susceptible than myocytes to oxidative stress following acute IRI but this injury can be reduced by HSPCs. (A) Flow cytometric gating strategy used for identifying oxidatively damaged (8-OHdG^{+}) ECs (CD31^{+} ; left) and myocytes (cTnT^{+} ; right) in digested whole hearts. **(B)** Percentage of each cell type obtained from a total of 30,000 events**.** A greater yield of myocytes is obtained (n=5; IR+HSPC groups n=4). **(C)** Endothelial ICAM-1 expression increases during ischaemia and further during reperfusion. This is reduced by HSPCs injected at the onset of reperfusion (*p<0.05 **p<0.01 vs sham; $^{+}$p<0.05 vs IR; Sidak; n=3). **(D)** Endothelial VCAM-1 expression does not increase during ischaemia but non-significantly increases during reperfusion. This is also reduced following HSPC administration (Sidak; n=3). **(E)** IRI, but not ischaemia alone, results in a significant endothelial oxidative damage which is reduced with HSPCs (**p<0.01 vs sham; $^{\#}$p<0.05 vs IR; Sidak; sham and ischaemia groups n=5; IR and IR+HSPC groups

n=4). **(F)** Oxidative damage in myocytes also increases but not to levels seen in endothelium (Sidak; n=5; IR+HSPC group n=4).

Figure 7. Microvascular endothelial oxidative stress can be reduced in VCECs in the presence of HSPCs *in vitro*. (A) Oxidative damage incurred by H_2O_2 treated vena cava endothelium is reduced following incubation with HSPCs for 72 hr (*p<0.05; n=4; t-test). **(B&C)** H_2O_2 driven ROS generation, measured by DHE staining, is reduced by HSPCs at 72hr (***p<0.001; n=3; t-test). Red = DHE stain; Yellow = CFSE-labelled HSPCs. Scale bars represent 100μm

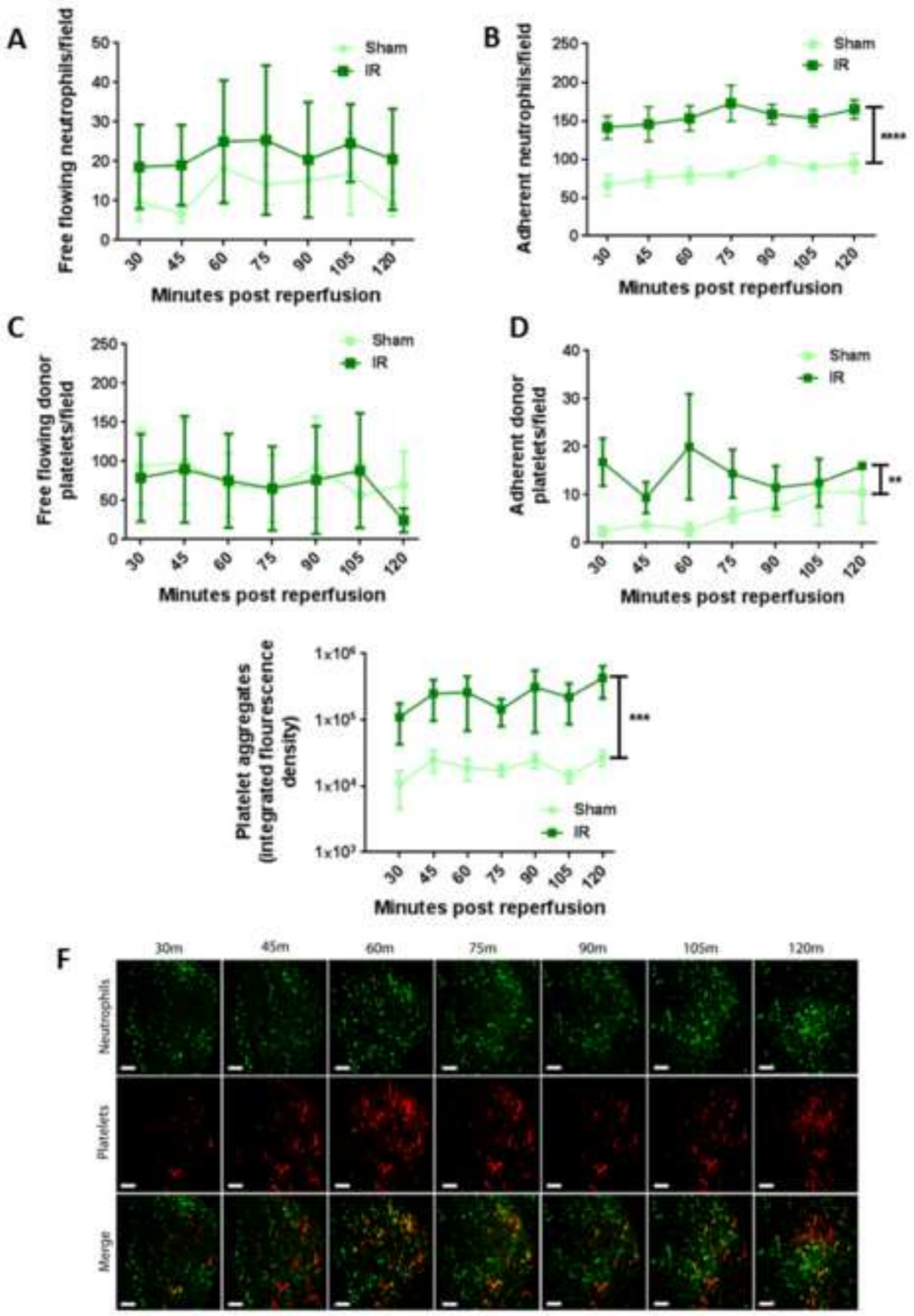

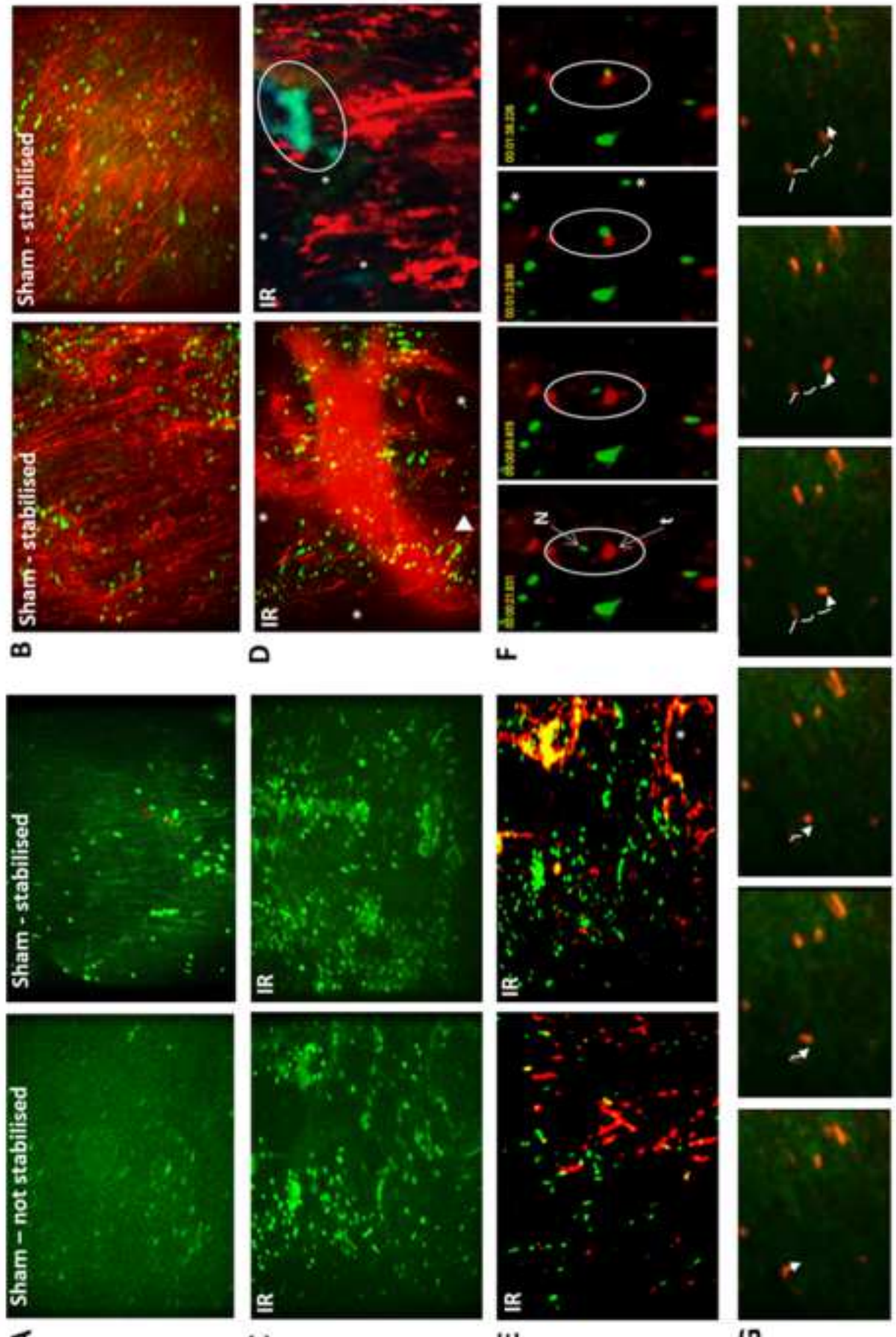

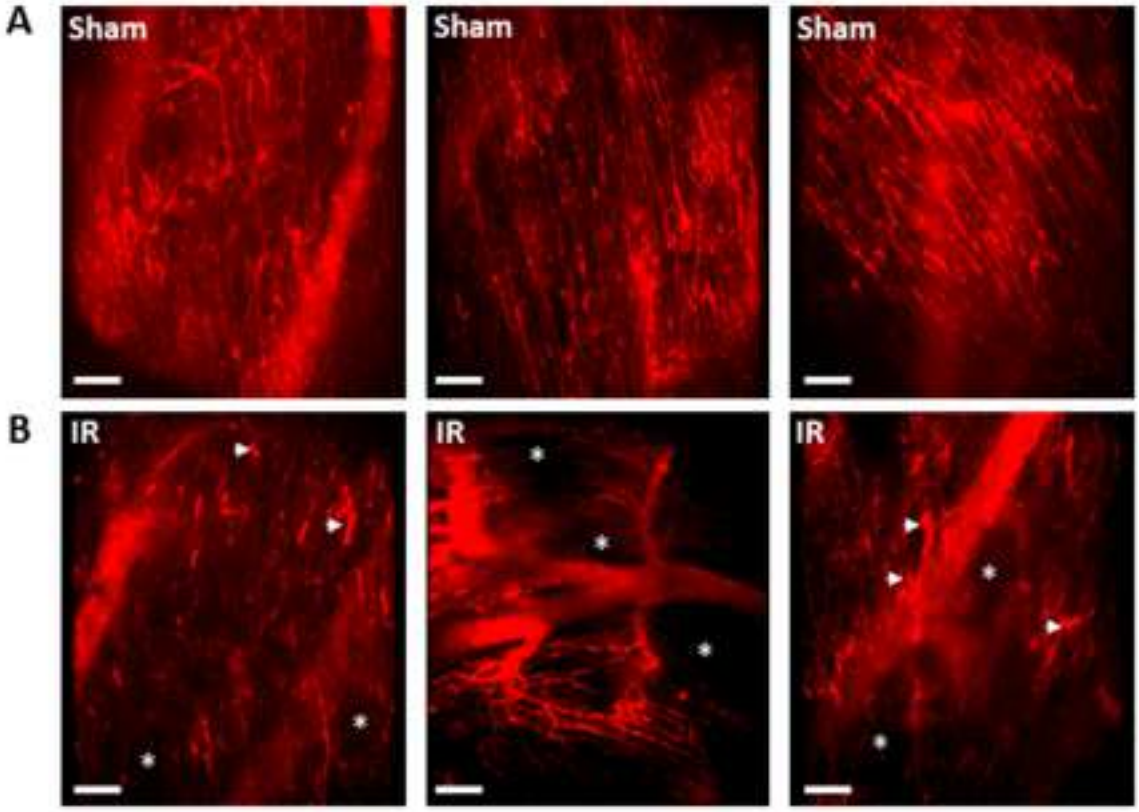

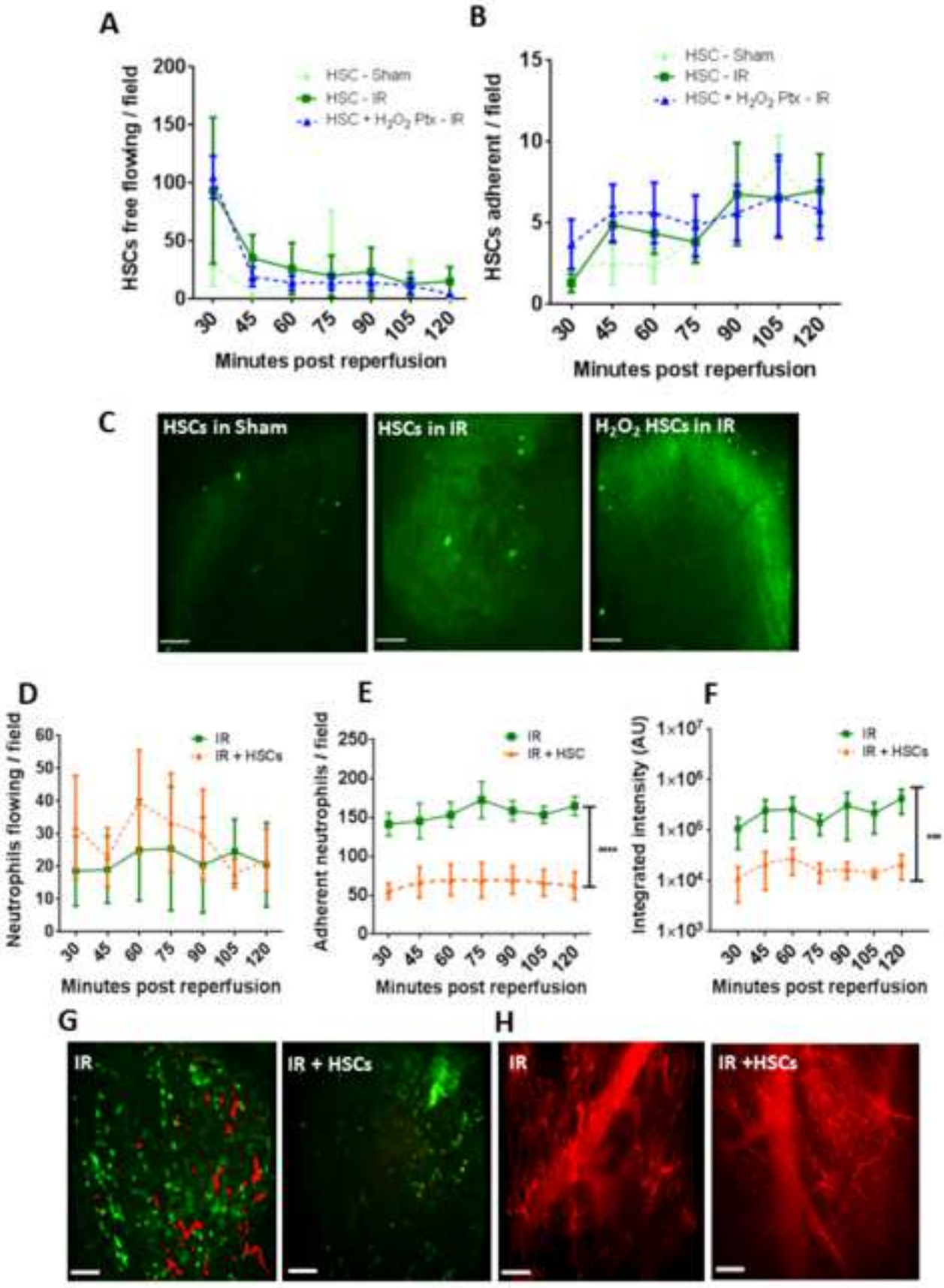

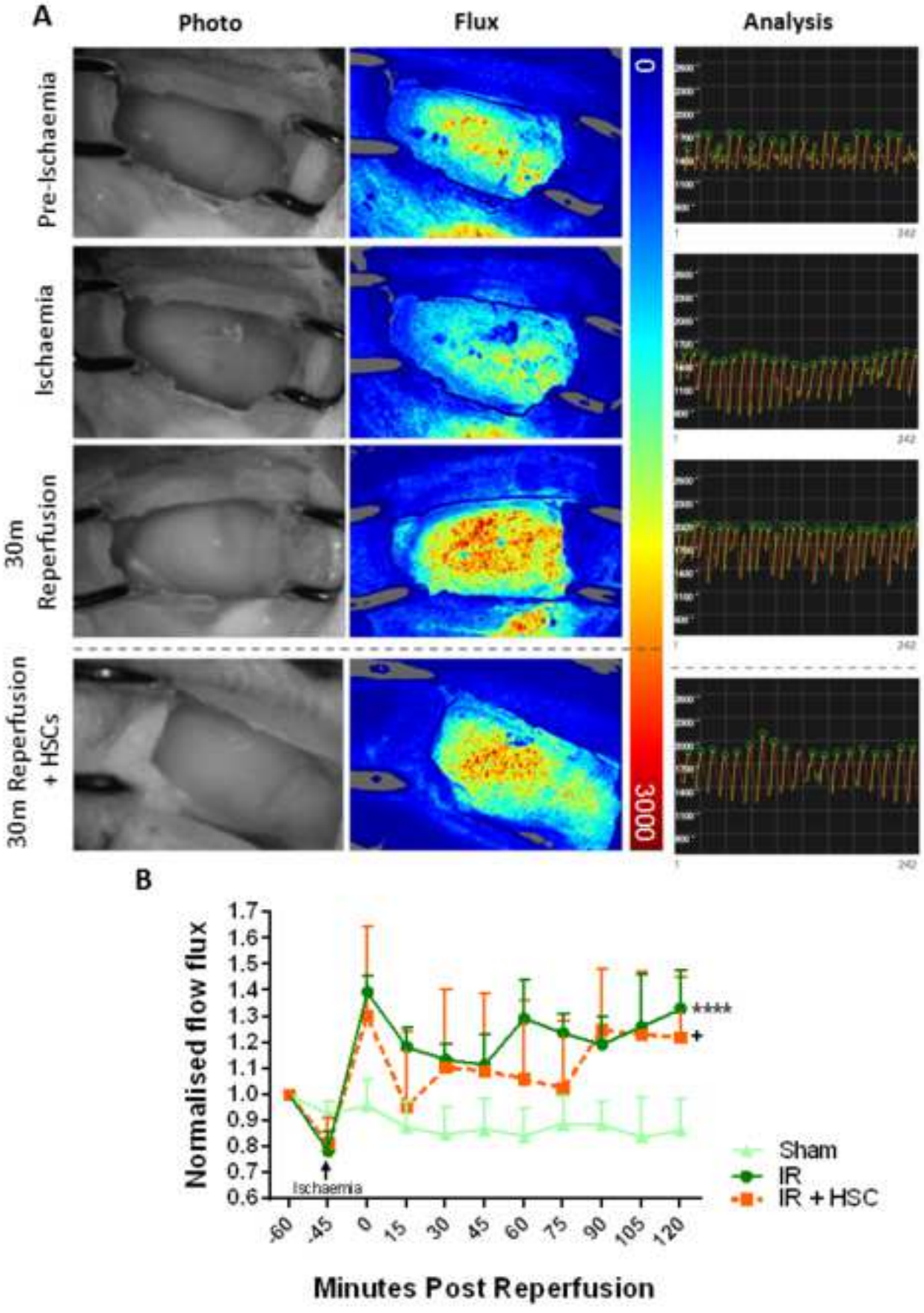

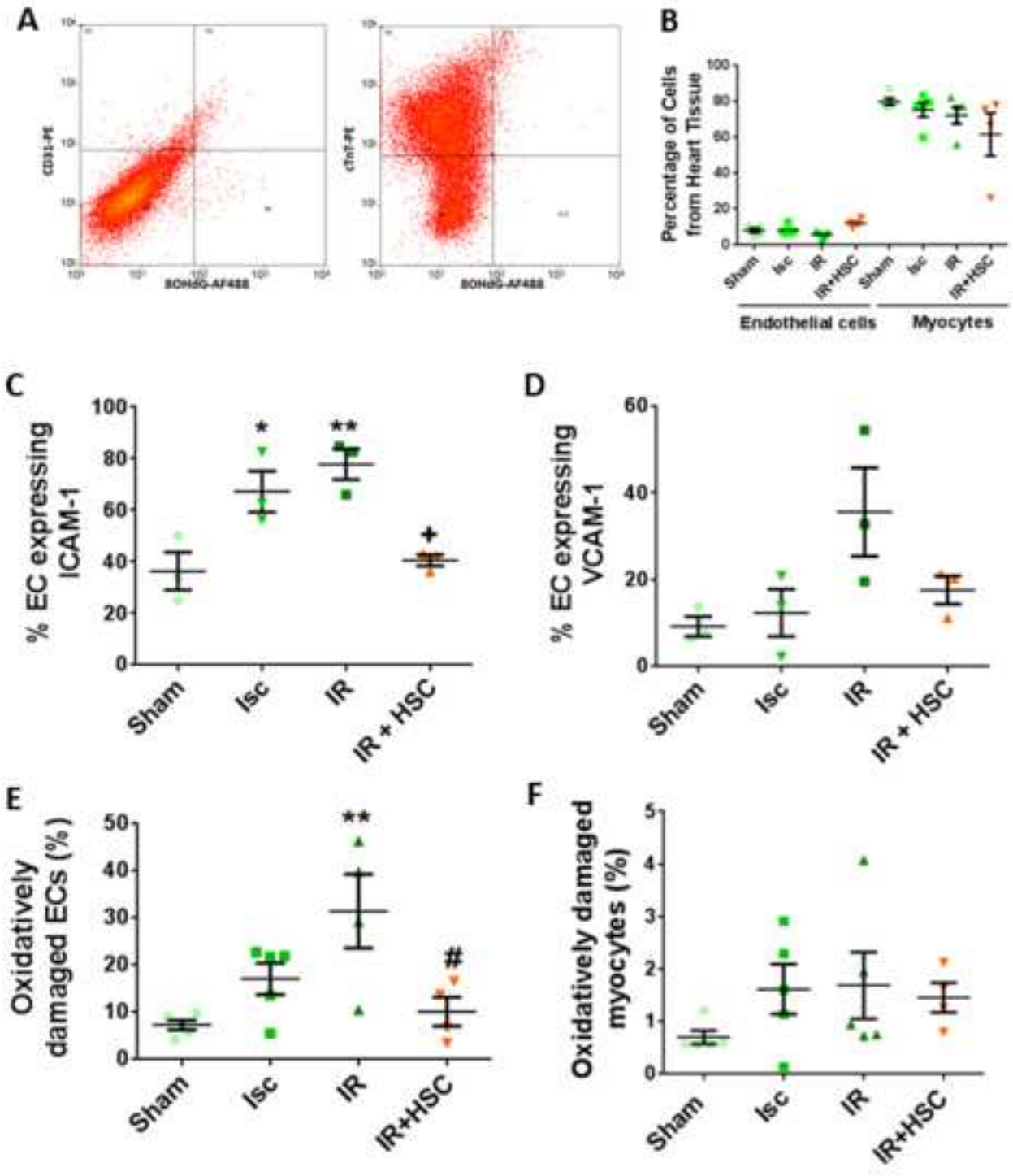

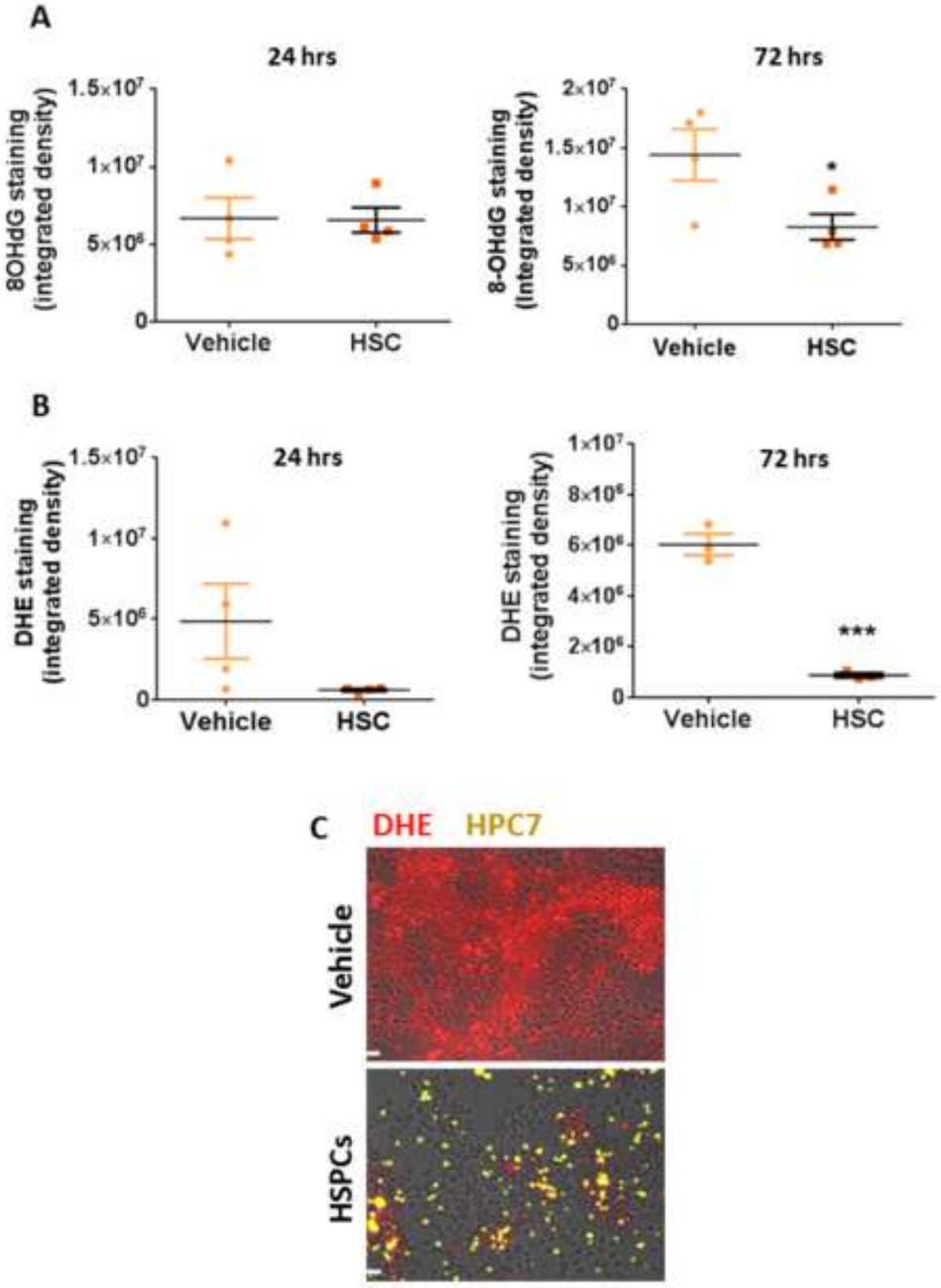

Graphical Abstract